11 Radionuclide Studies of the Lung

N.D. Greyson

Introduction

Nuclear medicine studies provide unique functional information based on the localizing properties of specific radiotracers in normal or pathologic processes. These images are complementary to conventional X-ray, computed tomography (CT), magnetic resonance imaging (MRI), and angiography, which offer highly detailed anatomy-based images of the lungs, pleura, and mediastinum. Radionuclide studies are noninvasive, widely available, and quantitative. These tests may obviate the need for interventional techniques such as angiography, biopsy, and bronchial alveolar lavage. They may be used in the detection and staging of malignancy, determining the activity of inflammatory processes, and in monitoring the response to therapy or progression of the disease, in a cost-effective, patient-tolerated manner.

Imaging Principles

Radiopharmaceuticals are molecules or compounds that contain a radioactive tracer. The distribution of the pharmaceutical in the body depends on its interaction with normal or pathologic tissues. Many different products are available for assessment of the respiratory system, including those that demonstrate regional ventilation, pulmonary artery perfusion, inflammation and sepsis, primary and secondary tumors, thrombus labeling, and alveolar–capillary permeability. Frequently, multiple studies, each reflecting different functional information, are used in combination.

The radioactive label permits external detection of the distribution of the pharmaceutical. Diagnostically useful radioisotopes are those whose unstable atom results in the emission of a gamma ray, or positron (positively charged electron). The site of this event can be detected using a gamma (or positron) camera, which maps out the distribution of radioactive emissions. The events are recorded and displayed, in planar, tomographic or three-dimensional format. Nuclear images that have relatively low spatial resolution, are "physiologic maps" rather than anatomic displays. They may be visually correlated or electronically merged with radiographs, for precise localization. Diagnosis is made by comparing the patient's results with the known normal localization of that radiopharmaceutical. The regional distribution of the tracer, and its changes over time may be quantified using computer analysis of regions of interest.

Techniques

Ventilation Imaging

Assessment of the patency of the airways is made using radiotracers that follow the ventilation pathways of least resistance to the level of the terminal bronchioles or alveoli. Xenon-133(^{133}Xe), an inert radioactive gas has been used, but it is now largely supplanted by aerosolized Technetium-99m labeled products.

Radioactive xenon ventilation studies are performed using a closed gas distribution system, charged with oxygen. The study is performed in three phases: an initial breath-hold following maximum inhalation of undiluted xenon gas; a 3–5 min equilibration achieved by rebreathing xenon mixed with oxygen; and a washout phase by breathing in room air, and breathing out xenon into a collecting reservoir for disposal. While this approach provides the most physiologic demonstration of airways patency, redistribution, and air-trapping, xenon gas is relatively expensive, and its long half-life produces significant radiation housekeeping difficulties. The dose of xenon gas must be purchased weekly in anticipation of the numbers of expected ventilation studies. This could result in wastage or insufficiency of supplies.

M. Sperber (ed.), *Radiologic Diagnosis of Chest Disease*

A radioactive aerosol is produced using an oxygen-driven nebulizing system containing a ^{99m}Tc-labeled product. Commonly ^{99m}Tc-diethylene triamine pentaacetic acid (DTPA) or ^{99m}Tc-sulphur colloid are used, but virtually any radiopharmaceutical may be nebulized for ventilation studies. This means that a cheap readily available product is always on hand. Aerosol ventilation may be carried out at normal tidal volume, without breath-holding, even on mechanically ventilated patients.

Aerosol particles less than 1.0 μm in diameter simulate a gas, passing through the airways of least resistance by laminar flow to the terminal bronchiole level. Normally there is very little adhesion of the particles to the mucosa of the proximal tracheobronchial tree, but in the terminal bronchioles and alveoli they stick to the cell surfaces. The activity remains in the lung for up to about 2 hrs, permitting imaging in multiple views. This offers an advantage over xenon studies, which are restricted to a single, usually posterior, set of images. Clearance of the aerosolized tracer is by mucocilliary action, absorption through the alveolar – capillary membrane, and by radioactive decay. The clearance time of soluble materials, such as ^{99m}Tc-DTPA is a measure of membrane permeability, and has been used as an indicator of alveolitis. The distribution of the aerosol also demonstrates the effectiveness of the delivery of aerosolized medication such as pentamidine.

The normal ventilation image (Fig. 11.1, upper row) shows symmetric activity in both lungs, with sharply defined pleural margins, costophrenic angles, diaphragmatic surfaces, cardiac silhouette and great vessels that match the usual contours seen on a chest radiograph. The scan usually demonstrates a normal gradient of ventilation, greater in the bases than in the apices.

In the presence of airways obstruction, or airspace disease, there is interference with the peripheral penetration of aerosol to the pleural surfaces. This results in inhomogeneous ventilation, with defects corresponding to the areas of hypoventilation (Fig. 11.2). With increased airways resistance, normal laminar flow is replaced by turbulence, causing the aerosol particles to stick to the airways walls at the site of obstruction. The resultant image shows "hot spots" at the level of obstruction (Fig. 11.3).

Perfusion Scanning

^{99m}Tc-labeled macroaggregates of human serum albumin (MAA), 10–60 μm in diameter, are larger than the pulmonary capillaries. When injected intravenously, they flow with the circulation through the right ventricle and pulmonary arteries, and into the pulmonary capillary bed. This results in their transient embolization in the pulmonary bed. To provide a wide margin of safety, approximately 300 000 particles are used in the injection, causing embolization of less than 0.1% of the precapillary arteriole bed (1). The albumin particles are metabolized and pass out of the capillary bed, with a clearance half time of less than 2 h. Although there are theoretical safety issues related to embolization of a compromised circulation such as in pulmonary hypertension or severe emphysema, possible right to left shunting causing micro-embolization of the systemic circulation, and protein allergy, in reality, significant side-effects are virtually never encountered.

A normal perfusion scan, performed in multiple views has features identical to the normal ventilation image (Fig. 11.1, lower row). Single or multiple areas of decreased perfusion may result from intraluminal obstruction (thrombus or other emboli, pulmonary artery stenosis, vasculitis), extrinsic compression (tumor, mediastinitis), destruction of the vascular bed (emphysema, bullae or abscess), vasospasm secondary to hypercapnea (associated with airspace consolidation, or bronchial obstruction), or vascular diversions (pulmonary arteriovenous malformation, right to left intrapulmonary or intracardiac shunts, postoperative pulmonary-to-systemic vascular anastomoses).

Perfusion abnormalities are characterized by their shape. "Vascular segment" perfusion defects are caused

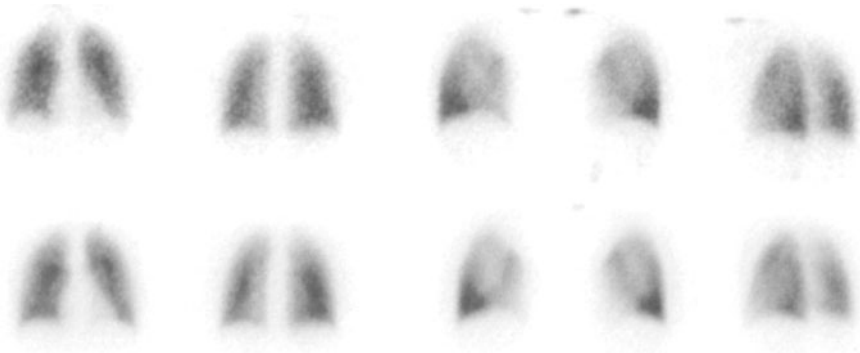

Figure 11.1. Normal ventilation (*upper row*) and perfusion (*lower row*) images. Of the 8 views normally obtained, anterior, posterior, right and left laterals, and the left posterior oblique views are shown. Ventilation and perfusion images match identically. Note the symmetry and homogeneity of activity, with a gradient of ventilation and perfusion favoring the lower lobes. The normal pleura, diaphragm, and cardiac outlines are well defined.

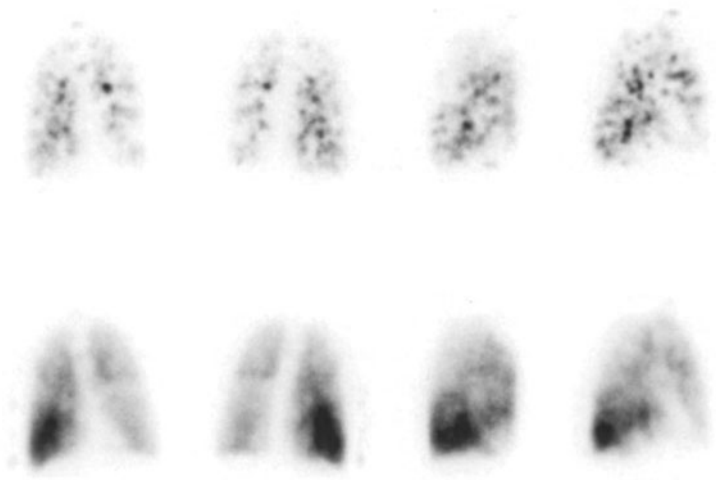

Figure 11.2. Emphysema. The ventilation images (*upper row*) show irregular patchy distribution of aerosol, with poor penetration to the periphery. The perfusion images (*lower row*) show nonsegmental, ill-defined defects. The ventilation pattern is worse than perfusion. There are no "vascular segment defects". This scan is a low probability for PE.

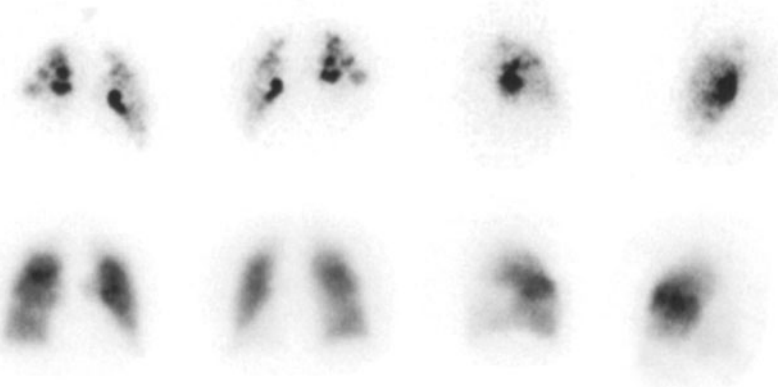

Figure 11.3. Obstructive lung disease. The ventilation images (*upper row*, anterior, posterior, right and left laterals), show very poor ventilation of the bases. The central "hot spots" indicate foci of local airways resistance, with partial obstruction and turbulent flow depositing the aerosol centrally. The perfusion images (*lower row*) show matched, but less severe, lower lobe defects. There are no "vascular segment defects". In conjunction with a clinical low pretest probability, and a normal venous Doppler, this patient has a low probability for PE. With higher probability clinical indications, this would be considered as an intermediate probability for PE, requiring further investigation.

by occlusion of a vessel, cutting off the blood supply to all distal branches. These defects are pleural-based, conical in three dimensions or triangular in two dimensions, usually with the apex directed toward the hilum. (Fig. 11.4). Recent vascular defects are usually so well defined that they can be named according to the lung segment involved. Vascular perfusion defects may be characterized by size (whole lung, lobar, segmental, or subsegmental).

"Nonsegmental" perfusion defects are usually less discrete, may cross segmental or pleural margins, and may not reach the pleural surface ("the peripheral stripe sign"). They may be explained by anatomic structures such as cardiomegaly, or a tortuous aorta, or by radiographic pathology such as pleural effusions ("the fissure sign"), consolidation, atelectasis, or obstructive lung disease (Figs. 11.2, 11.3). Vascular redistribution to the upper zones in congestive heart failure reverses the normal gradient which favors the lower lobes.

The ventilation scan is performed first, followed by the injection of MAA for the perfusion scan. A larger dose of activity bound to MAA is administered compared with the inhaled aerosol. Thus the perfusion pattern is not affected by the activity of the preceding ventilation phase. Gamma camera imaging of both studies is performed in the same positions, so that any perfusion defects may be compared with the ventilation of the same anatomic segment.

Gallium Scanning for Sepsis and Tumor

Gallium-67 citrate (^{67}Ga) is an analog of the ferric ion. Thus it binds preferentially to transferrin, ferritin, and lactoferrin, as well as less avid binding to albumin and other proteins. Gallium also reacts with phosphate, resulting in mild bone localization. A normal gallium scan demonstrates the distribution of iron and albumin stores, with preference to those organs high in lactoferrin, as well

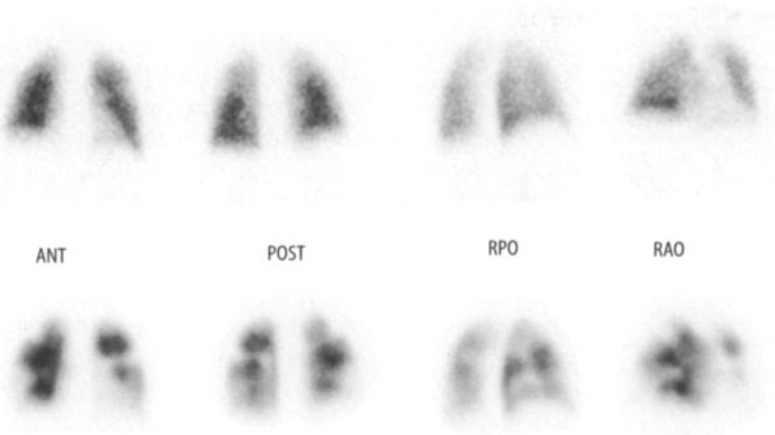

Figure 11.4. Pulmonary emboli. The ventilation images (*upper row*) are normal. The perfusion images (*lower row*) show multiple matched, moderate-sized, bilateral vascular segment shaped perfusion defects. This patient has a high probability for PE, regardless of the clinical presentation. Only primary pulmonary hypertension, vasculitis, or old unresolved PE would produce a similar pattern. *ANT*, anterior; POST, posterior; *RPO*, right pulmonary obstruction; *RAO*, right aortic obstruction.

as some skeletal uptake (Fig. 11.5). Normally, there is no visible pulmonary or mediastinal uptake.

Septic or aseptic inflammation, and malignancy may have increased vascularity, which enhances the delivery of the gallium to the abnormal area. Increased vascular permeability permits the protein-bound gallium to exit the capillary bed, and bind to abnormal proteins associated with inflammation or tumor. Gallium also binds onto bacterial and white blood cell walls. Phagocytosis results in intracellular accumulation of gallium, which then binds to lysosomes, which are more plentiful in inflammatory or tumor cells.

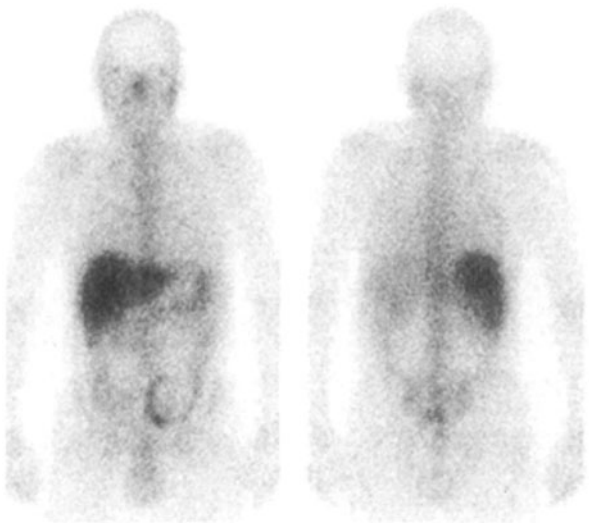

Figure 11.5. Normal ^{67}Ga-citrate scan. Anterior and posterior views. There is normal activity in the liver, faint bone uptake, some bowel excretion, minimal salivary and lachrymal uptake, and diffuse soft tissue appearance. There is no demonstrable uptake in the lungs, or mediastinum.

Similar mechanisms occur in both neoplasm and inflammation. Thus a positive scan cannot differentiate between these lesions. Gallium uptake may be considered as a bioassay of the activity of a known inflammatory process (acute versus chronic or quiescent inflammation; response of sepsis to treatment, etc.) (2). Low grade, well-differentiated tumors often have lower gallium affinity ("false negative"), which is a good prognostic sign (3). A good theraputic response will result in lower gallium uptake in tumors inflammation.

Tumour Localization

Fluorine-18 Deoxyglucose (FDG) Imaging by Positron Emission Tomography (PET)

Deyxoglucose labeled with fluorine-18 (^{18}F) is a sensitive detector of cellular metabolism (4). FDG is a glucose analog that follows the phosphorylation pathways, but becomes fixed within the cells prior to ATP production. The degree of accumulation is indicative of the rate of glycolysis or cellular metabolism, and is used in oncology to differentiate benign from malignant lesions, to detect primary tumors and metastases, and to follow response to therapy. Some false-positive results occur in focal inflammatory conditions because of increased local metabolism associated with sepsis and repair.

The detection of FDG requires a special camera, able to image the very high energy pair of photons produced when a positron reacts with an electron. The short half-life of ^{18}F (1.8 h) requires proximity to the cyclotron production facility. It is a relatively expensive product, and not as widely available as gamma-emitting radiopharmaceuticals.

Thallium-201 and ^{99m}Tc-labeled Perfusion Agents

Thallium-201 (^{201}Tc) in the form of thallous chloride is a potassium analog. ^{99m}Tc labeled sestamibi (Cardiolite, Dupont Pharmaceuticals Company), and ^{99m}Tc-labeled tetrofosmin (Myoview, Nycomed Amersham) are lipophilic cations. These radiotracers are widely used in assessment of myocardial perfusion however, they have been found to localize in neoplasms. This uptake is proportional to the tumor blood flow, but is also related to the intracellular concentration of mitochondria. The increased negative electrical charge on the mitochondria of neoplastic cells causes the fixation of the positively charged cations.

Monoclonal Antibodies and Peptides

Localization of the radiotracer may be accomplished by the use of specially formulated antibodies directed against specific tumor cells, platelets, or various proteins. Also, tailor-made peptide chains that simulate the binding site of antibodies or hormones may be used to target specific receptors for these agents in tumors or thrombi.

Clinical Applications

Pulmonary Embolism

Ventilation-Perfusion Imaging

Pulmonary embolic disease is a potentially life-threatening occurrence, particularly in immobilized patients, following surgery, or in individuals with deep vein thrombophlebitis. Clinical signs and symptoms are frequently nonspecific (5) and radiographic findings are often absent or nondiagnostic. As pulmonary embolism (PE) is a common comorbid factor, or a direct cause of death, and is a frequent incidental finding at post mortem, it is often misdiagnosed and undertreated. Ventilation – perfusion imaging remains a keystone test in the diagnosis of PE, in conjunction with other noninvasive techniques such as venous Doppler ultrasound, and D-dimer assay. Contrast angiography, either by direct intrapulmonary artery injection (6), or helical CT (7–9) may help to give a more specific diagnosis, particularly in the more proximal branches.

The ventilation–perfusion lung scan is not a "pulmonary embolism scan". It identifies the presence and extent of ventilation and/or perfusion abnormalities, the interpretation of which is used in risk stratification of patients with suspected pulmonary embolism.

Many large clinical trials, such as PIOPED (10–12), and PISA-PED(13), have reviewed the patterns of ventilation–perfusion imaging in patients with suspected PE. The probability of PE was retrospectively based on analysis of these patterns and follow-up of the patients.

PE classically shows-vascular segment-shaped perfusion defects, in areas of normal ventilation (Fig. 11.4) (except when transient bronchospasm is present, or in the presence of consolidation due to infarction, or atelectasis). A normal ventilation – perfusion scan essentially excludes PE, and it is safe to withhold further diagnostic tests, and treatment (14,15). A high probability lung scan (80–95% prevalence of PE) is found in patients with lung scans that show one or more large defects, or multiple medium-sized vascular segment-shaped perfusion defects in areas with normal ventilation and no corresponding radiographic changes. In these patients treatment may be commenced on the base of the scan and a high clinical pretest probability. Absent perfusion of a whole lung may rarely be due to a massive proximal or saddle thrombus, but it is more commonly due to obstruction of the pulmonary artery by malignancy, or intracardiac or intrapulmonary shunts.

"Intermediate probability" scans carry a significant prevalence of emboli (but wide range, from 20% to 80%). These scans show small or moderate-sized perfusion defects with normal ventilation and normal radiographs, or perfusion defects with matched with consolidation, particularly in the lower zones. This category essentially includes any pattern that is not clearly "normal," "high probability," or low probability" for PE (12). To assess the need for treatment in these patients, results must be considered in light of the clinical presentation, the pretest probability of emboli, interpretation of the radiographic findings, venous Doppler, and the D-dimer test.

"Low probability scans" (less than 10% prevalence) demonstrate nonsegmental defects; abnormalities associated with radiographic lesions not suggestive of emboli, or a few very small (less than 25% of a named pulmonary segment) perfusion defects, or perfusion defects smaller than matching radiographic abnormalities, and multiple-mated ventilation and perfusion defects with a normal radiograph (12). Low probability scans exclude significant-sized emboli and have a very low mortality if untreated (16).

"Very low probability" (< 5% prevalence of PE) is associated with very small defects, and a normal radiograph.

The ventilation – perfusion lung scan is a relatively sensitive detector of abnormalities, but it is not specific in the detection of PE. Nevertheless it is still the key diagnostic test to determine the need for immediate treatment, further diagnosis, or dismissal. In the original PIOPED study (10), which relied heavily on the scan pattern, and less on other factors, an abnormal scan was 98% sensitive but only 10% specific for emboli. A high probability scan was 87% specific for PE but occurred in only 40% of PE

patients. There was a large number of indeterminate scans, and emboli were present in 14% of low probability studies. Thus, unless the perfusion is absolutely normal, PE cannot be ruled out solely by the scan.

Many modifications to the PIOPED criteria have been proposed (12, 17, 18). The addition of pretest probabilities, and knowledge of specific high risk clinical indicators and ancillary testing, have significantly reduced the number of equivocal reports, with more definitive interpretations that are clinically useful in risk stratification (19). Intermediate or indeterminate categories carry a wide range of probability for PE . In the clinical setting of immobilization, lower extremity trauma, recent surgery, and central venous instrumentation, a defect has a higher likelihood of PE (20). A defect in a patient with known underlying cardiopulmonary disease is less likely to be a PE case (21).

Consistent reporting terminology is necessary to ensure appropriate communication with the referring clinicians (22–25). This facilitates treatment, and avoids expensive, unnecessary or invasive procedures.

Thrombus-Seeking Techniques

The optimistic search for reliable and readily available thrombus-seeking agents, will hopefully convert the diagnosis of pulmonary embolism from the interpretation of a defect to the direct identification of a thrombus (Fig. 11.6). There is an almost unlimited variety of potential thrombus-localizing radiopharmaceuticals. These include radiolabeling the constituents of a thrombus, such as platelets, thrombin, fibrin, or fibrinogen; labeled monoclonal antibodies against various thrombus components; labeled peptide chains to bind onto receptor sites on thrombi or their breakdown products; and labeled thrombolytic agents, such as plasmin, urokinase, streptokinase etc. (26–37). However, despite such an extensive potential list, and many decades of research, no one product has emerged as an agent of choice. A completely occluding thromboembolism may not have a sufficiently large surface exposed to the bloodstream to permit interaction of the radiopharmaceutical with the thrombus. False-negative studies may occur in older thrombi that have lost their active thrombogenic characteristics. Some agents are sensitive but not specific, giving false-positive localization in inflammatory sites.

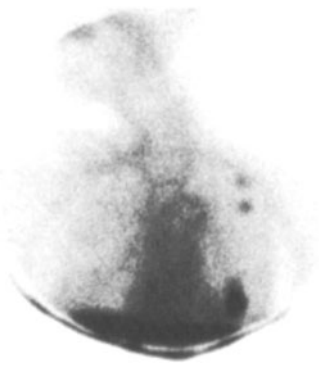

Figure 11.6. Positive identification of PE by ^{99m}Tc-labeled plasmin. Thrombi in the left upper lung, and lingula, adjacent to the left ventricle apex, corresponded to perfusion defects on the lung scan. There was also uptake in several thrombi located in deep venous thrombosis in legs. (Provided courtesy of the Department of Nuclear Medicine, Toronto General Hospital.)

Inflammatory Conditions

Gallium Scanning in Pneumonitis

The lung is susceptible to numerous infectious and non-infectious inflammatory processes, most with conspicuous changes on radiographs or lung CT. Active infections are usually recognizable by clinical signs and symptoms, but radiographic abnormalities often persist even after the acute process has subsided, leaving fibrosis, chronic infiltrates, or granulomas. Many aseptic inflammatory conditions such as fibrosing alveolitis, sarcoidosis, allergic pneumonitis, pneumoconioses, and drug toxicity reactions may undergo a chronic and relapsing sequence, and tuberculosis may recur in previously scarred areas. Conventional radiography and CT may have difficulty in identifying the active component.

The most common radionuclide test for evaluation of the activity of an inflammatory process is the use of ^{67}Ga-citrate. Areas of both septic and aseptic inflammation will show increased localization of gallium in active sites. Areas of fibrosis do not accumulate gallium, whereas areas of active alveolitis, active tuberculosis, sarcoidosis, or *Pneumocystis carinii* pneumonia (PCP) indicate the activity of the disease, and its distribution, but not its cause. Sequential studies will show progression or response to treatment (38).

The intensity of gallium uptake may be semiquantitatively assessed by comparing the intensity of lung uptake with that of neighboring organs. The normal gallium appearance, shows no significant pulmonary uptake (Fig. 11.5). In early inflammation (grade 1), the heart is a "cold" object relative to mild lung uptake, and the pulmonary activity in the chest is greater than the subdiaphragmatic activity. Lung intensity exceeds the thoracic soft tissues in grade 2, the sternum or other bony structures (grade 3), and, finally, has greater uptake than in the liver (grade 4) (Fig. 11.7). The intensity of gallium uptake correlates well with the cellularity of the aspirate obtained by bronchoalveolar lavage (39), but there is also increased uptake in the acellular supernatant fraction of the BAL in PCP (40).

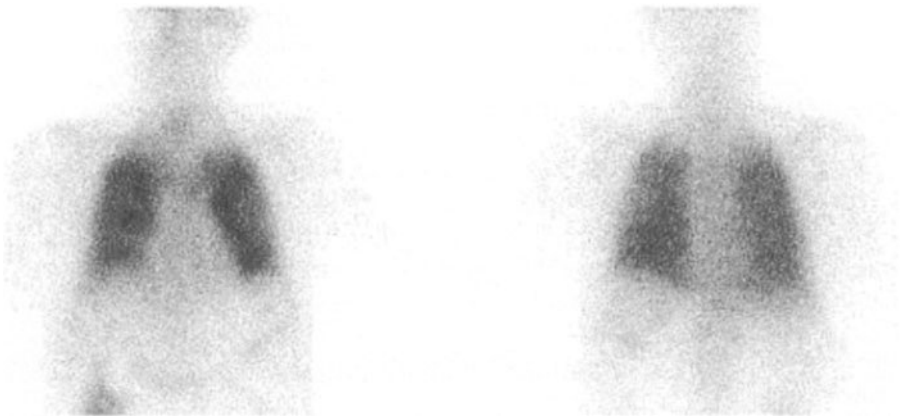

Figure 11.7. Pneumocystis carinii pneumonia. ^{67}Ga scan, anterior and posterior views. Diffuse bilateral increased activity. Grade 4 uptake (lung hotter than the liver), in this patient with AIDS.

HIV and AIDS-Related Diseases

Patients who are immunosuppressed due to human immunodeficiency virus (HIV) infection, steroids, post-transplantation, or have marrow replacement diseases are vulnerable to opportunistic infections. Up to 80% of these patients experience PCP, but this complication may be may be radiographically nonspecific, or even occult, in 50% of patients (41). The gallium scan in these patients will show increased lung activity, indicating the active inflammatory process. The usual pattern is diffuse, homogeneous, bilateral, markedly increased uptake. The response to treatment with pentamidine is indicated by normalization of the gallium scan. However, aerosolized pentamidine may not reach some areas as effectively. Some patients on prophylactic pentamidine who develop PCP may have gallium uptake in only part of the lung (42) making the diagnosis less specific (43). Accelerated clearance of ^{99m}Tc-DTPA aerosol is also demonstrated in the active phase of PCP.

Tuberculosis or atypical tuberculosis causes focal gallium uptake in lymph nodes, or focal distribution within the parenchyma, or other affected sites This appearance is in contrast to the usual diffuse pulmonary uptake pattern of PCP infection.

Kaposi sarcoma may be a complication in one third of acquired minute deficiency syndrome (AIDS) patients. Radiographically, sarcoma in the lungs may not be differentiated from inflammatory infiltrates. It has been shown, however, that Kaposi sarcoma is almost always gallium negative. PCP, tuberculosis or other bacterial pneumonia, and/or Kaposi sarcoma may be present within a nonspecific parenchymal infiltration. On the gallium scan the area of Kaposi sarcoma will be negative, while the other inflammatory processes will be positive. Kaposi sarcoma can be further confirmed by positive uptake within the tumor by thallium or sestamibi scanning, while inflammatory lesions generally have absent uptake by these agents (44,45).

^{67}Ga is also a sensitive marker of non-Hodgkin lymphoma. A whole-body scan may be used to stage the distribution of this malignancy.

Sarcoidosis

Gallium is highly sensitive in locating areas of active sarcoidosis. A whole-body gallium scan will reveal the distribution of active intrathoracic and systemic sarcoid lesions. The usual patterns include the pulmonary parenchyma, hilar or peripheral adenopathy, salivary and lachrymal uptake, cutaneous uptake in erythema nodosum, liver and spleen infiltration, and intracranial neural uptake. Intrathoracic uptake of gallium may be diffuse or patchy in the lung parenchyma, or within mediastinal and/or peritracheal lymph nodes, or combined. Regretably, the uptake of gallium is nonspecific and cannot differentiate the hilar adenopathy of sarcoidosis from lymph node involvement by lymphoma. However, in sarcoidosis, the common mediastinal lymph node pattern involves the peritracheal and perihilar lymph nodes in a distribution suggesting the Greek letter lambda (λ). In the presence of the sicca syndrome, or uveoparotitis, the salivary and lachrymal uptake produce an appearance reminiscent of the face of a panda. The combination of the "lambda" and "panda" signs (Fig. 11.8) is virtually exclusive to sarcoidosis, and not seen in lymphoma (46,47). In lymphoma, peripheral lymph node involvement is more common (48).

Cancer Detection and Staging

The principle means of detection of lung malignancies is by plain film or chest CT. However, it may not be possible to differentiate a benign from malignant process within a pulmonary nodule or an enlarged lymph node. Metastases

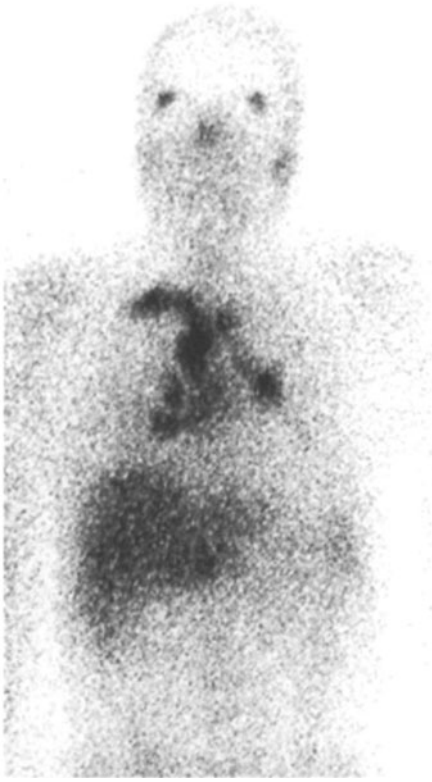

Figure 11.8. Sarcoidosis. Anterior gallium scan shows the classic "lambda sign" (λ) of perihilar and peritracheal lymph node uptake of ^{67}Ga. This patient also shows the "panda sign" of increased lachrymal and salivary gland uptake. The sign is actually misnamed, as a panda has black ears, not black cheeks.

and tumor invasion may be difficult to differentiate from nonmalignant granulomas, postsurgical scarring, or post-radiation fibrosis, or they may be obscured by normal mediastinal structures (Fig. 11.9). Histologic sampling may produce specific diagnoses, but not all patients, nor all nodules are, amenable to intervention. The use of tumor-seeking radiotracers, particularly ^{18}F-FDG, is now becoming widely used for improved detection of primary and metastatic malignant lesions, and for localization of a site for biopsy (49,50). The therapeutic regimen depends on tumor staging. The positive FDG scan helps to select patients for surgery, radiation or chemotherapy (51–53). Detection of tumor spread usually directs the patient away from further surgical intervention (54). Follow-up FDG PET scans may demonstrate response to treatment, or progression of disease.

FDG is expensive, requires special imaging detectors, and the 1.8 h half-life may make it logistically difficult for centers who do not have direct access to a cyclotron. However, the cost efficacy of this technique in preventing unnecessary thoracotomies is now well established (55). Gamma cameras are now available, which may be used for both routine gamma ray nuclear medicine studies, as well as positron detection by dual head coincidence imaging, in those institutions that do not require a dedicated positron camera.

^{67}Ga, which is much cheaper and readily available, has been used for lung cancer detection (56,57). However, it may not be able to resolve lesions less than 2 cm in diameter (versus 0.5 cm for PET imaging), and has variable uptake in many tumor cell types. It is still useful in staging of lymphoma (Fig. 11.9).

Thallium, sestamibi and tetrofosmin localize in a variety of tumors (58–61). The uptake of sestamibi and tetrofosmin involves similar pathways of intracellular penetration as various chemotheraputic agents. Lack of uptake of these tracers by malignant tumors correlates with the presence of P-glycoprotein, a factor in multidrug resistance (MDR) to various chemotherapeutic agents. These radiopharmaceuticals may demonstrate the presence of MDR, and predict the possible failure of certain therapeutic regimens (62–64).

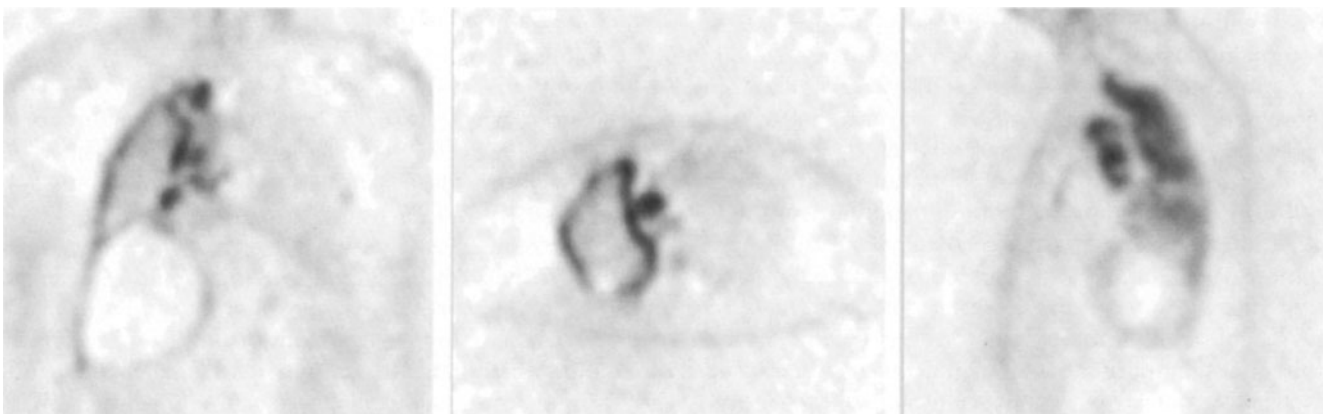

Figure 11.9. ^{18}F FDG PET in malignant mesothelioma. Coronal (**a**), transaxial (**b**), and sagittal (**c**) tomographic images show marked uptake around the right lung, and in several metastatic foci in right hilar nodes. (Courtesy of the Department of Nuclear Medicine, McMaster University Medical Centre, Hamilton, Canada.)

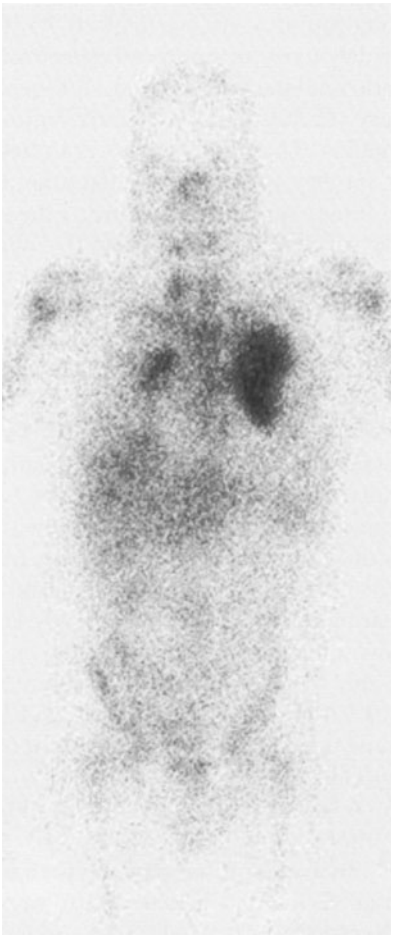

Figure 11.10. Non-Hodgkin lymphoma. Anterior ^{67}Ga scan showing avid uptake in a left lung pulmonary infiltrate, right hilar node, right supraclavicular node, and tiny foci in the liver.

Aerosol Clearance in Alveolitis

Following the administration of ^{99m}Tc-labeled DTPA by aerosol inhalation, there is gradual resorption of this material through the alveolar capillary membrane, into the blood stream, with a normal clearance half-time of more than 60 min (1% per minute). Healthy smokers have an accelerated clearance (4% per minute). In patients with alveolitis, inhalation or radiation pneumonitis, PCP and other infectious processes, sarcoidosis, vasculitis pneumoconiosis, etc., the clearance half-time is markedly accelerated (up to 8% per minute), due to increased capillary permeability and increased porosity of the alveolar epithelial membrane (65–69). An accelerated clearance, even before radiographic changes, is predictive of the possible future development of adult respiratary distress syndrome (ARDS), prompting early therapy (69). It may be used to monitor the progress, or response to treatment of patients who have alveolitis.

Radiation Safety

The clinically useful radiopharmaceuticals are designed to minimize radiation dose. Short-lived tracers are preferred, and isotopes with alpha or beta particle decay are avoided when possible. The radiation burden to the patient depends on the physical decay rate of the tracer (physical $T_{1/2}$), and the duration of the radiopharmaceutical retained in the body (biologic $T_{1/2}$). Combined, these produce the "effective half-time".

Although ^{133}Xe has a long 5 day physical $T_{1/2}$, it is eliminated from the body within minutes of inhalation. Thus it results in a very minimal radiation dose (70). ^{67}Ga however, has a 3 day physical $T_{1/2}$, and prolonged binding and storage. The potentially high radiation dose is compensated by using a relatively low administered quantity, compared with ^{99m}Tc, which has a 6h $T_{1/2}$. Nuclear medicine studies have an acceptably low radiation dose, in the order of that used in fluoroscopy, spine radiographs, and CT, which results in an insignificant addition to the naturally occurring cancer rate (70).

Pulmonary embolism may be suspected in some pregnant patients, justifying a ventilation – perfusion lung scan. Some radiation dose to the fetus is inevitable, but for the radiopharmaceuticals used in lung scans, this is less then or equal to to the annual natural background radiation exposure (70). Radiation at such low levels does not produce any measurable increase in the incidence of fetal malformations or other complications of pregnancy, compared with the significant incidence of spontaneous genetic problems and miscarrings (71). The hazards of nondiagnosis of a pulmonary embolism, or the inappropriate use of anticoagulants results in a much higher risk of complications than the theoretical effects of these low levels of radiation (72,73).

However, pregnant patients have concerns, and should be counseled about the relative risks of having, or not having, the test. A signed consent to having the test should be obtained. To further offer psychologic support (but probably negligible additional biologic safety), to the pregnant patient, the attending physicians, and ourselves, we may reduce the dose of administered radiopharmaceutical by as much as 50%, and double the imaging time.

Many radioisotopes are excreted in milk in small amounts (74). If a nuclear scan is required during lactation, the mother should be advised that when short-lived tracers such as ^{99m}Tc are used, nursing should be deferred for 24 h. The breast may be pumped and the milk-discarded. For longer-lived radioisotopes, particularly gallium, which binds to lactoferrin, nursing should probably be discontinued completely, as there will be activity in the milk for 1–2 weeks.

Patients may have some residual radiation in their bodies at the conclusion of the diagnostic test. Natural radiation decay accounts for most of the subsequent loss,

and some is eliminated in the urine or stool. While the radiation is measurable by sensitive detectors, patients are not considered to be any hazard to the general public or to their family. As a conservative precaution they may wish to remain apart from small children for a day or so, as if they had a cold or the, flu.

Summary

A wide variety of nuclear medicine techniques are available to diagnose and monitor embolic, inflammatory and neoplastic pulmonary conditions. The specific functional information depends on the type of tracer used. Although nuclear images have low spatial resolution they provide a unique physiologic map of metabolic processes occurring in the body which is complementary to the anatomic structural imaging provided by other modalities. Nuclear medicine images are acquired digitally and are thus intrinsically quantitative. This quantitative evaluation may be useful for sequential assessment.

Reference

1. Davis MA, Taube RA (1978) Pulmonary perfusion imaging: Acute toxicity and safety factors as a function of particle size. J Nucl Med 19:1209–1213.
2. Myslivecek M, Husak V, Kolek V, et al. (1992) Absolute quantification of gallium-67 citrate accumulation in the lungs and its importance for the evaluation of disease activity in pulmonary sarcoidosis. Eur J Nucl Med 19:1016–1022.
3. Lentle BC, Catz Z, Dierich HC, et al. (1987) Gallium-67 scintigraphy and non-small-cell bronchogenic carcinoma: A quantitative in-vivo predictive assay? Can Med Assoc J 137:815–817.
4. Brown RS, Leung JY, Kison PV, et al. (1999) Glucose transporters and FDG uptake in untreated primary human non-small cell lung cancer. J Nucl Med 40:556–565.
5. Kemp PM, Tarver DS, Batty V, et al. (1996) Pulmonary embolism. Is the clinical history a useful adjunct to aid the interpretation of the equivocal scan? Clin Nucl Med 21:203–207.
6. van Beek EJ, Reekers JA, Batchelor DA, et al. (1996) Feasibility, safety and clinical utility of angiography in patients with suspected pulmonary embolism. Eur Radiol 6:415–419.
7. Garg K, Welsh CH, Feyerabend AJ, et al. (1998) Pulmonary embolism: Diagnosis with spiral CT and ventilation–perfusion scanning – correlation with pulmonary angiographic results or clinical outcome. Radiology 208:201–208.
8. Robinson PJ (1996) Ventilation-perfusion lung scanning and spiral computed tomography of the lungs: Competing or complementary modalities? Eur J Nucl Med 23:1547–1553.
9. Goodman LR, Curtin JJ, Mewissen MW, et al. (1995) Detection of pulmonary embolism in patients with unresolved clinical and scintigraphic diagnosis: Helical CT versus angiography. AJR 164:1369–1374.
10. The PIOPED Investigators (1990) Value of the ventilation/perfusion scan in acute pulmonary embolism. Results of the prospective investigation of pulmonary embolism diagnosis (PIOPED). JAMA 263:2753–2759.
11. Gottschalk A, Sostman HD, Coleman RE, et al. (1993) Ventilation–perfusion scintigraphy in the PIOPED study. Part II. Evaluation of the scintigraphic criteria and interpretations. J Nucl Med 34:1119–1126.
12. Worsley DF, Alavi A (1995) Comprehensive analysis of the results of the PIOPED study. J Nucl Med 36:2380–2387.
13. Miniati M, Pistolesi M, Marini C, et al. (1996) Value of perfusion lung scan in the diagnosis of pulmonary embolism: Results of the prospective investigative study of acute pulmonary embolism diagnosis (PISA-PED). Am J Respir Crit Care Med 154:1387–1393.
14. van Beek EJ, Kuyer PM, Schenk BE, et al. (1995) A normal perfusion lung scan in patients with clinically suspected pulmonary embolism. Frequency and clinical validity. Chest 108:170–173.
15. Hull RD, Raskob GE, Coates G, et al. (1990) Clinical validity of a normal perfusion lung scan in patients with suspected pulmonary embolism. Chest 97:23–26.
16. Rajendran JG, Jacobson AF (1999) Review of 6-month mortality following low-probability lung scans. Arch Intern Med 159:349–352.
17. Freitas JE, Sarosi MG, Nagle CC, et al. (1995) Modified PIOPED criteria used in clinical practice. J Nucl Med 36:1573–1578.
18. Stein PD, Relyea B, Gottschalk A (1996) Evaluation of individual criteria for low probability interpretation of ventilation–perfusion lung scans. J Nucl Med 37:577–581.
19. Freeman L (1996) The low probability V/Q lung scan: Can its credibility be enhanced? (Editorial). J Nucl Med 37:582–584.
20. Worsley DF, Palevsky HI, Alavi A (1994) A detailed evaluation of patients with acute pulmonary embolism and low-or very-low-probability lung scan interpretations. Arch Intern Med 154: 2737–2741.
21. Stein PD, Gottschalk A, Henry JW, et al. (1993) Stratification of patients according to prior cardiopulmonary disease and probability assessment based on the number of mismatched segmental equivalent perfusion defects. Approaches to strengthen the diagnostic value of ventilation–perfusion lung scans in acute pulmonary embolism. Chest 104:1461–1467.
22. Gray HW, McKillop JH, Bessent RG (1993) Lung scan reports: Interpretation by clinicians. Nucl Med Commun 14:989–994.
23. Gray HW, McKillop JH, Bessent RG (1993) Lung scan reporting language. What does it mean? Nucl Med Commun 14:1084–1087.
24. Kember PG, Euinton HA, Morcos SK (1997) Clinicians' interpretation of the indeterminate ventilation – perfusion scan report. Br J Radiol 70:1109–1111.
25. Kaboli P, Buscombe JR, Ell PJ (1993) Reporting ventilation –perfusion lung scintigraphy: Impact on subsequent use of anticoagulation therapy. Postgrad Med J 69:851–855.
26. Knight LC (1993) Scintigraphic methods for detecting vascular thrombus. J Nucl Med 34(Suppl3):554–561.
27. Dewanjee MK (1987) Methods of assessment of thrombus in vivo. Ann NY Acad Sci 516:541–571.
28. Som D, Oster ZH (1994) Thrombus-specific imaging: Approaching the elusive goal. J Nucl Med 35:202–203.
29. Higashi S, Kuniyasu Y (1984) An experimental study of deep-vein thrombosis using ^{99m}Tc-fibrinogen. Eur J Nucl Med 9:548–552.
30. Smyth JV, Dodd PD, Walker MG (1995) Indium-111 platelet scintigraphy in vascular disease. Br J Surg 82:588–595.
31. Knight LC (1988) Imaging thrombi with radiolabelled fragment E1. Nucl Med Commun 9:849–857.
32. Lavender JP, Stuttle AW, Peters AM, et al. (1988) In vivo studies with an anti-platelet monoclonal antibody: P256. Nucl Med Commun 9:817–822.
33. Lister-James J, Knight LC, Mamer AH, et al. (1996) Thrombus imaging with a Technetium-99m-labelled activated platelet receptor-binding peptide. J Nucl Med 37:775–781.
34. Ciavolella M, Tavolaro R, Di Loreto M, et al. (1999) Immunoscintigraphy of venous thrombi: Clinical effectiveness of a new antifibrin D-dimer monoclonal antibody. Angiology 50:103–109.
35. Deacon JM, Ell PJ, Anderson P, et al. (1980) Technetium 99m-plasmin: A new test for the detection of deep vein thrombosis. Br J Radiol 53:673–677.

36. Millar WT, Smith JF (1974) Localization of deep-venous thrombosis using technetium-99m-labelled urokinase. Lancet 2:695–696.
37. Kempi V, Van Der Linden W, Von Scheele C (1974) Diagnosis of deep vein thrombosis with 99mTc-streptokinase: A clinical comparison with phlebography. Br Med J 4:748–749.
38. Kao CH, Lin HT, Yu SL, et al. (1994) Lung inflammation in patients with systemic lupus erythematosus detected by quantitative ^{67}Ga-citrate scanning. Nucl Med Commun 15:928–931.
39. Line BR, Fulmer JD, Reynolds HY, et al. (1978) Gallium-67 citrate scanning in the staging of idiopathic pulmonary fibrosis: Correlation with physiological and morphological features and bronchoalveolar lavage. Am Rev Respir Dis 118:355–365.
40. Smith RL, Berkowitz KA, Lewis ML (1992) Pulmonary disposition of gallium-67 in patients with Pneumocystis pneumonia: An analysis using bronchoalveolar lavage. J Nucl Med 33:512–515.
41. Barron T, Birnbbaum N, Shane L, et al. (1987) Pneumocystis carinii pneumonia studied by gallium-67 scanning. Radiology 164:791–793.
42. Katial R, Honeycutt W, Oswald S (1994) Pneumocystis carinii pneumonia presenting as focal bibasilar uptake on galium scan during aerosolized pentamidine prophylaxis. J Nucl Med 35:1038–1040.
43. Kramer EL (1994) PCP, AIDS and nuclear medicine (Editorial). J Nucl Med 35:1034–1037.
44. Abdel-Dayem H, Bag R, DiFabrizio L, et al. (1996) Evaluation of sequential thallium and gallium scans of the chest in AIDS patients. J Nucl Med 37:1662–1667.
45. Turoglu HT, Akisik MF, Naddaf SY, et al. (1998) Tumor and infection localizaton in AIDS patients: Ga-67 and Tl-201 findings. Clin Nucl Med 23:446–459.
46. Sulavik SB, Spencer RP, Palestro CJ, et al. (1993) Specificity and sensitivity of distinctive chest radiographic and/or ^{67}Ga images in the noninvasive diagnosis of sarcoidosis. Chest 103:403–409.
47. Sulavik SB, Spencer RP, Weed DA, et al. (1990) Recognition of distinctive patterns of gallium-67 distribution in sarcoidosis. J Nucl Med 31:1901–1914.
48. Israel HL, Albertine KH, Park CH, et al. (1991) Whole-body gallium 67 scans. Role in diagnosis of sarcoidosis. Am Rev Respir Dis 144:1182–1186.
49. Chiti A, Schreiner FA, Crippa F, et al. (1999) Nuclear medicine procedures in lung cancer. Eur J Nucl Med 26:533–555.
50. Inoue T, Kim EE, Komaki R, et al. (1995) Detecting recurrent or residual lung cancer with FDG-PET. J Nucl Med 36:788–793.
51. Steinhart HC, Hauser M, Allemann F, et al. (1997) Non-small cell lung cancer: Nodal staging with FDG-PET versus CT with correlative lymph node mapping and sampling. Radiology 202:441–446.
52. Scott WJ, Schwabe JC, Gupta NC, et al. (1994) Positron emission tomography of lung tumours and mediastinal lymph nodes using F18-fluorodeoxyglucose. Ann Thorac Surg 58:698–703.
53. Guhlmann A, Storck M, KotzerkeJ, et al. (1997) Lymph node staging in non-small cell lung cancer: Evaluation by [^{18}]FDG positron emission tomography (PET). Thorax 52:438–441.
54. Bury T, Dowlati A, Paulus P, et al. (1996) Staging of non-small cell lung cancer by whole-body fluorine-18 deoxyglucose positron emission tomography. Eur J Nucl Med 23:204–206.
55. Gambhir SS, Hoh CK, Phelps ME, et al. (1996) Decision tree sensitivity analysis for cost-effectiveness of FDG-PET in the staging and management of non-small cell lung carcinoma. J Nucl Med 37:1428–1436.
56. Ragheb AM, Elgazzar AH, Ibrahim AK, et al. (1995) A comparative study between planar Ga-67, Tl-201 images, chest x-ray, and x-ray CT in inoperable non-small cell carcinoma of the lung. Clin Nucl Med 20:426–433.
57. Matsuno S, Tanabe M, Kawasaki Y, et al. (1992) Effectiveness of planar images and single photon emission tomography of thallium-201 compared with gallium-67 in patients with primary lung cancer. Eur J Nucl Med 19:86–95.
58. Takekawa H, Takaoka K, Tsukamoto E, et al. (1997) Thallium-201 single photon emission computed tomography as an indicator of prognosis for patients with lung carcinoma. Cancer 80:198–203.
59. Greyson ND, Freeman M (1998) Incidental detection of a malignant thymic tumor by Tc-99m sestamibi cardiac imaging. Clin Nucl Med 23:781–782.
60. Arbab AS, Koizumi K, Toyama K, et al. (1996) Uptake of technetium-99m-tetrofosmin, technetium-99m-MIBI and thallium-201 in tumor cell lines. J Nucl Med 37:1551–1556.
61. Bom HS, Kim YC, Song HC, et al. (1998) Technetium-99m-MIBI uptake in small cell lung cancer. J Nucl Med 39:91–94.
62. Piwnica-Worms D, Chiu ML, Budding M, et al. (1993) Functional imaging of multidrug-resistant P-glycoprotein with an organotechnetium complex. Cancer Res 53:977–984.
63. Ballinger JR, Bannerman J, Boxen I, et al. (1996) Technetium-99m-tetrofosmin as a substrate for P-glycoprotein: In vitro studies in a multidrug-resistant breast tumor cells. J Nucl Med 37:1578–1582.
64. Basoglu T, Bernay I, Coskun C, et al. (1998) Pulmonary Tc-99m tetrofosmin imaging: Clinical experience with detecting malignant lesions and monitoring response to therapy. Clin Nucl Med 23:753–757.
65. Coates G, O'Brodovich (1986) Measurement of pulmonary epithelial permeability with 99mTc-DTPA aerosol. Semin Nucl Med 16:275–284.
66. Susskind H, Weber DA, Lau YH, et al. (1997) Impaired permeability in radiation-induced lung injury detected by technetium-99m-DTPA lung clearance. J Nucl Med 38:966–971.
67. Susskind H. Rom WN (1992) Lung inflammation in coal miners assessed by uptake of ^{67}Ga-citrate and clearance of inhaled ^{99m}Tc-labeled diethylenetriamine pentaacetate aerosol. Am Rev Respir Dis 146:47–52.
68. Jacobs MP, Baughman RP, Hughes J, et al. (1985) Radioaerosol lung clearance in patients with active pulmonary sarcoidosis. Am Rev Respir Dis 131:687–689.
69. Tennenberg SD (1987) The use of ^{99m}Tc-DTPA radioaerosol lung clearance in the assessment of acute lung injury: clinical applicability in the adult respiratory distress syndrome. Respir Care 32:757–772.
70. Committee 3 of the International Commission on Radiation Protection (1993) Summary of the current ICRP principles for protection of the patient in nuclear medicine. Pergamon Press, Oxford.
71. Ritenour ER (1986) Health effects of low level radiation: Carcinogenesis, teratogenesis, and mutagenesis. Semin Nucl Med 16:106–117.
72. Sorenson JA (1986) Perception of radiation hazards. Semin Nucl Med 16:158–170
73. van Beek EJ, Kuijer PM, Buller HR, et al. (1997) The clinical course of patients with suspected pulmonary embolism. Arch Intern Med 157:2593–2598.
74. Ahlgren L, Ivarsson S, Johansson L, et al. (1985) Excretion of radionuclides in human breast milk after the administration of radiopharmaceuticals. J Nucl Med 26:1085–1090.